Earth, Planets and Space

FULL PAPER Open Access

A simplification of rigorous atmospheric raytracing based on judicious rectilinear paths for near-surface GNSS reflectometry

Thalia Nikolaidou[1*], Marcelo Santos[1], Simon D. P. Williams[2] and Felipe Geremia-Nievinski[3]

Abstract

Atmospheric delays are known to cause biases in Global Navigation Satellite System Reflectometry (GNSS-R) altimetry applications, such as for sea-level monitoring. The main quantity of interest is the reflection-minus-direct or interferometric atmospheric delay. Recently, we have presented a rigorous raytracing procedure to account for linear and angular refraction in conjunction with reflection as observed from near-surface platforms. Here, we demonstrate the feasibility of simplifying the ray trajectory by imposing a rectilinear wave propagation model. Two variants were assessed, based on the apparent or refracted satellite direction on the one hand and the geometric or vacuum conditions on the other hand. The former was shown to agree with rigorous results in terms of interferometric radio length while the latter agreed in terms of the interferometric vacuum distance. Upon a judicious combination of the best aspects of the two rectilinear cases, we have defined a mixed variant with excellent agreement with rigorous raytracing in terms of interferometric atmospheric delay. We further showed that mapping functions developed for GNSS positioning cannot be reused for GNSS-R purposes without adaptations. Otherwise, the total atmospheric delay may be underestimated by up to 50% at low elevation angles. The present work facilitates the adaptation of existing atmospheric raytracing software for GNSS-R purposes.

Keywords: GPS, GNSS, GNSS-R, Reflectometry, Atmospheric delay, Atmospheric refraction, Ray-tracing, Radio wave propagation

Introduction

Global Navigation Satellite System Reflectometry (GNSS-R) (Cardellach et al. 2011; Jin et al. 2014; Zavorotny et al. 2014) has been widely demonstrated for long-term ground-based coastal sea level altimetry (Larson et al. 2013; 2017). Atmospheric refraction is known to cause a propagation delay which produces a bias in GNSS-R altimetry, depending on the satellite elevation angle and the reflector height. Almost all assessments of GNSS-R against co-located tide gauges ignore a constant offset between the two sensors, except for example Santamaría-Gómez et al. (2015); this in part is not only due to the lack of leveling (surveying) across the two locations but also due to the atmospheric bias. Unfortunately, this limitation undermines one of the promoted advantages of GNSS-R altimetry, of providing geocentric sea level measurement. Besides a constant offset (average error), systematic atmospheric refraction errors found in sea level retrievals versus satellite elevation angle (Williams and Nievinski 2017) also affect the precision of retrievals when forming a site-wide average sea level across all visible satellites.

Under multipath reception conditions, direct and reflected radio waves are separated by the interferometric propagation delay $\tau_i = \tau_r - \tau_d$ (Nievinski and Larson 2014). Under the hypothesis of a large flat and horizontal reflector surface in vacuum, and ignoring

*Correspondence: Thalia.Nikolaidou@unb.ca
[1] Department of Geodesy and Geomatics Engineering, University of New Brunswick, Fredericton, Canada
Full list of author information is available at the end of the article

other effects, the interferometric propagation delay can be expressed as $\tau_i = 2H \sin e$ where e is the satellite elevation angle and H is the reflector height, i.e., the vertical distance between the receiver and the reflecting surface. It is the interferometric atmospheric delay which needs to be removed in GNSS-R for determining unbiased reflector height.

Atmospheric refraction manifests in both speed retardation and direction bending along the propagating ray (Nilsson et al. 2013). Its linear and angular components are combined, resulting in the atmospheric propagation delay, which affects GNSS observables such as signal-to-noise ratio (SNR), pseudo-range and carrier phase. In altimetry, the atmospheric delay may be understood as it were causing a mirage effect, in which the reflecting surface appears to be higher than where it actually is.

Several studies have recognized the importance of atmospheric refraction errors in GNSS-R altimetric retrievals (Anderson 2000; Treuhaft et al. 2001; Fabra et al. 2012; Semmling et al. 2012; Roussel et al. 2014; Santamaría-Gómez and Watson 2017; Williams and Nievinski 2017). To address the issue, some authors have suggested the adoption of mapping functions used in GNSS positioning, developed for line-of-sight or direct propagation from satellites (Nafisi et al. 2012) with minimal adaptation for GNSS-R applications. For example, Cardellach et al. (2011) states that "*…the delays induced by the tropospheric layer above the receiving platform cancel out, and only those due to the bottom layer, between the surface and the receiver, affect the altimetric range…*" In line with this concept of a vertically partitioned atmosphere, Zavorotny et al. (2014) state that "*Only the effect coming from the troposphere below the receiver needs to be corrected.*" A similar assumption is held in Treuhaft et al. (2001), who defined the zenith delay difference (across surface and antenna altitudes) and multiplied it by a direct mapping function.

However, models for direct propagation as used in GNSS positioning may adequately capture only the effect of linear refraction, i.e., that of speed retardation. This is because the angular refraction experienced by incoming rays in the upper atmospheric layer (i.e., in the portion above the antenna) does not necessarily cancel out when forming the interferometric atmospheric delay, even for near-surface configurations (Santamaría-Gómez and Watson 2017). The incoming reflection ray deviates from a straight line as a function of the gradient of refractivity along its entire path; it is thus a cumulative effect, not restricted to the lower portion of the atmosphere, i.e., between the receiver and the reflecting surface.

As the incident ray arrives along the apparent satellite elevation angle, and abiding to Snell's law, the refracted reflection point will be shifted compared to unrefracted atmospheric conditions. As the baseline or reference condition for comparison is that of propagation in vacuum, angular refraction thus causes an additional atmospheric delay of geometric nature (Santamaría-Gómez and Watson 2017).

In Nikolaidou et al. (2020), we have unified the linear and angular components of interferometric atmospheric delay experienced in GNSS-R, demonstrating how they can be derived from first principles. We have also explained the twofold effect of ray bending, introducing sub-components of the atmospheric geometric delay, to express the shifting of the reflection point as well as the deviation of the ray from a straight line. In that work, we have analyzed the bent wave propagation in ground-based GNSS-R altimetry applications. We used a rigorous raytracing approach (RI) in which the Eikonal equation was solved for determining the ray trajectory. Results were of high fidelity but somewhat opaque about the refraction effects involved.

Here, we demonstrate a simplified raytracing approach to determine the interferometric atmospheric delay. We show that the large-scale atmospheric geometric delay can be well captured by a judicious choice of rectilinear raypaths. We then assess, for varying satellite elevation and receiver height, under what observation conditions small-scale atmospheric geometric delay is negligible. We justify the simplified rectilinear modeling because it was a common approximation in previous GNSS studies, such as in water–vapor GNSS tomography (Rohm and Bosy 2009; Bender et al. 2011). It was also very common in early modeling efforts of atmosphere effects in radio propagation (Hopfield 1969; Saastamoinen 1972).

In Sect. "Interferometric Raytracing", we describe the numerical procedure while in Sect. "Atmospheric Delay Modeling" we lay down a model for the interaction between the various quantities. An alternative formulation is also presented in Sect. "Atmospheric Delay Modeling", based on the atmospheric layer between receiving antenna and reflecting surface. Numerical assessment results are shown and discussed in Sect. "Results and Discussion", while Sect. "Conclusions" concludes the paper with a summary of the main findings.

Interferometric raytracing

Figure 1 depicts the setup involved in a refracted reflection as observed from a near-surface receiver. The main position vectors refer to an arbitrary ray position, $\boldsymbol{r}$; transmitting satellite, $\boldsymbol{r}_{\text{sat}}$; receiving antenna, $\boldsymbol{r}_{\text{ant}}$; vacuum surface reflection point, $\boldsymbol{r}_{\text{sfc}}$; and refracted reflection point, $\boldsymbol{r}'_{\text{sfc}}$. Viewing directions are denoted as unit vectors such as $\Delta\hat{\boldsymbol{r}}_{\text{sat}}$ and $\Delta\hat{\boldsymbol{r}}'_{\text{sat}}$ for geometric (vacuum) and apparent (refracted) conditions, respectively.

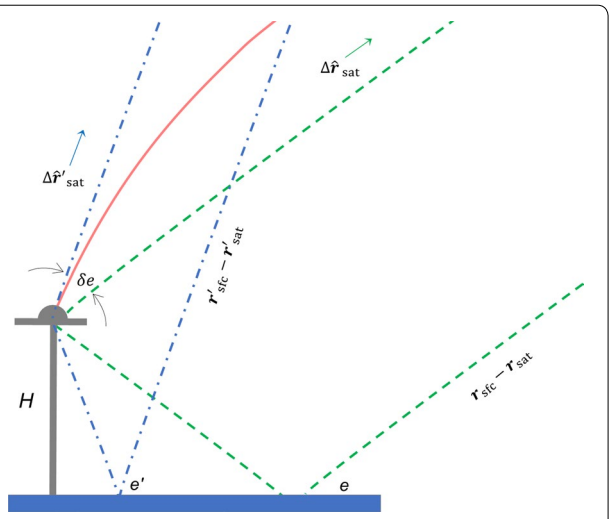

Fig. 1 Geometry of the two rectilinear approaches: rectilinear-geometric (green dashed line) and rectilinear-apparent (blue dash-dot line)

Rigorous raytracing

A rigorous interferometric raytracing procedure has been developed in a previous study (Nikolaidou et al. 2020), where we gave a detailed description of both the direct and reflection raytracing. The background can be summarized as follows.

We assume a spherical atmosphere, where the spatial gradient of the index of refraction (∇n) points to the center of the sphere and the raypath is a plane curve, i.e., there is no out-of-plane bending:

$$\hat{\nabla} n = \frac{\nabla n}{\|\nabla n\|} = -\hat{\mathbf{r}}' = -\frac{\boldsymbol{r}'}{\|\boldsymbol{r}'\|} \tag{1}$$

where $\boldsymbol{r}' = \boldsymbol{r} - \boldsymbol{r}_o$ is a ray vector position with respect to the center of the sphere; the sphere is said to osculate the Earth's ellipsoid, i.e., its center $\boldsymbol{r}_o$ lies along the ellipsoidal normal and has radius equal to the ellipsoidal Gaussian radius of curvature (Nievinski and Santos 2010).

The evolution of the ray is defined by solving the Eikonal equation (Born and Wolf 1999):

$$\frac{\partial}{\partial l}\left(n\frac{\partial \boldsymbol{r}}{\partial l}\right) = \nabla n \tag{2}$$

With n the (scalar) field of index of refraction and l the incremental raypath arc length. On the one hand, linear refraction will slow down the radio wave (via the atmospheric speed of propagation $v = c/n$, where c is the vacuum speed of light). On the other hand, angular refraction will change the direction of propagation, via the gradient of refraction ∇n (Nievinski and Santos 2010).

To solve Eq. (2), a set of conditions needs to be specified. Often the time is reversed so that raytracing starts at the receiving antenna and ends near the transmitting satellite. A common set of conditions is made of an initial position and an initial direction—the receiver position and the satellite apparent direction; in this case, the final position (the satellite position) is determined as a consequence of the raytracing procedure. Another common choice of boundary conditions is made of initial and final positions (receiver and satellite positions); in this case, the initial or apparent direction follows from raytracing. We start by raytracing the direct ray followed by the reflection. The latter is performed separately for each of the incident and scattered legs (incoming and outgoing segments), which split the whole reflection ray at the specular point. For more details, the reader is referred to Nikolaidou et al. (2020).

Rectilinear raytracing

We simplified the rigorous bent raypath, based on the Eikonal equation, by postulating rectilinear radio propagation:

$$\boldsymbol{r} = \check{\boldsymbol{r}} + s \cdot \hat{\boldsymbol{t}}. \tag{3}$$

So, rays are artificially set to coincide with straight line segments, where $\check{\boldsymbol{r}}$ is the initial ray position, $\hat{\boldsymbol{t}}$ the ray tangent direction (constant unit vector), and s the incremental ray distance.

Under this simplified model, the solution of initial- and boundary-value problems is no longer necessary, as the ray trajectory is completely known in advance. We denote the infinitesimal straight line distance as ds, e.g., $\|\boldsymbol{r}_2 - \boldsymbol{r}_1\| = \int_{\boldsymbol{r}}^{\boldsymbol{r}_2} ds$. A numerical quadrature is retained, to integrate the propagation delays d based on refractivity $N \equiv n - 1$: $d = \int N ds$. Propagation still occurs in an inhomogeneous atmospheric model so the ray is subject to linear refraction and, indirectly, may also be subject to angular refraction, depending on the postulated ray direction, as detailed below.

There are two variants of the rectilinear model. For the *rectilinear geometric* (RG) model, the direct ray is based on the satellite and antenna position in vacuum:

$$\mathrm{RG_d}: \begin{cases} \check{\boldsymbol{r}}_d = \boldsymbol{r}_{\text{ant}} \\ \hat{\boldsymbol{t}}_d = \Delta\hat{\boldsymbol{r}}_{\text{sat}} \end{cases} \tag{4}$$

where the geometric or vacuum satellite relative direction with respect to the antenna is

$$\begin{aligned}\Delta\hat{\boldsymbol{r}}_{\text{sat}} &= \frac{\Delta\boldsymbol{r}_{\text{sat}}}{\Delta r_{\text{sat}}}\\ \Delta r_{\text{sat}} &= \|\Delta\boldsymbol{r}_{\text{sat}}\|\\ \Delta\boldsymbol{r}_{\text{sat}} &= \boldsymbol{r}_{\text{sat}} - \boldsymbol{r}_{\text{ant}},\end{aligned} \tag{5}$$

Continuing with the RG model, the reflection is specified in terms of its incoming and outgoing parts:

$$\text{RG}_{\text{r/inc}} : \begin{cases} \check{\boldsymbol{r}}_{r/\text{inc}} = \boldsymbol{r}_{\text{sfc}} \\ \hat{\boldsymbol{t}}_{r/\text{inc}} = \Delta\hat{\boldsymbol{r}}_{\text{sat}} \end{cases} \tag{6}$$

$$\text{RG}_{\text{r/out}} : \begin{cases} \check{\boldsymbol{r}}_{r/\text{out}} = \boldsymbol{r}_{\text{sfc}} \\ \hat{\boldsymbol{t}}_{r/\text{out}} = -\Delta\hat{\boldsymbol{r}}_{\text{sfc}} \end{cases} \tag{7}$$

where the geometric or vacuum relative surface direction with respect to the antenna is

$$\begin{aligned}\Delta\hat{\boldsymbol{r}}_{\text{sfc}} &= \frac{\Delta\boldsymbol{r}_{\text{sfc}}}{\Delta r_{\text{sfc}}}\\ \Delta\text{r}_{\text{sfc}} &= \|\Delta\boldsymbol{r}_{\text{sfc}}\|\\ \Delta\boldsymbol{r}_{\text{sfc}} &= \boldsymbol{r}_{\text{sfc}} - \boldsymbol{r}_{\text{ant}}\end{aligned} . \tag{8}$$

The second variant of this simplified ray model is the *rectilinear apparent* (RA) model, for which the direct ray is defined as

$$RA_d : \begin{cases} \check{\boldsymbol{r}}_d = \boldsymbol{r}_{\text{ant}} \\ \hat{\boldsymbol{t}}_d = \Delta\hat{\boldsymbol{r}}'_{\text{sat}} \end{cases} . \tag{9}$$

The antenna position $\boldsymbol{r}_{\text{ant}}$ is unchanged and the apparent or refracted satellite relative direction with respect to the antenna $\Delta\hat{\boldsymbol{r}}'_{\text{sat}}$ is assumed known; in practice, the latter is obtained from a previous rigorous direct-path raytracing (Nikolaidou et al. 2020). The RA reflection is again specified in terms of its incoming and outgoing parts:

$$\text{RA}_{\text{r/inc}} : \begin{cases} \check{\boldsymbol{r}}_{r/\text{inc}} = \boldsymbol{r}'_{\text{sfc}} \\ \hat{\boldsymbol{t}}_{r/\text{inc}} = \Delta\hat{\boldsymbol{r}}'_{\text{sat}} \end{cases} \tag{10}$$

$$\text{RA}_{\text{r/out}} : \begin{cases} \check{\boldsymbol{r}}_{r/\text{out}} = \boldsymbol{r}'_{\text{sfc}} \\ \hat{\boldsymbol{t}}_{r/\text{out}} = -\Delta\hat{\boldsymbol{r}}'_{\text{sfc}} \end{cases} \tag{11}$$

where the apparent or refracted relative surface position with respect to the antenna, $\Delta\hat{\boldsymbol{r}}'_{\text{sfc}}$ is obtained analogously to $\Delta\hat{\boldsymbol{r}}'_{\text{sat}}$. Where necessary, we establish a fictitious *apparent satellite position* as

$$\boldsymbol{r}'_{\text{sat}} = \boldsymbol{r}_{\text{ant}} + D_d \cdot \Delta\hat{\boldsymbol{r}}'_{\text{sat}} \tag{12}$$

lying along a given apparent satellite direction $\Delta\hat{\boldsymbol{r}}'_{\text{sat}}$ at a direct distance $D_d = \left\|\Delta\hat{\boldsymbol{r}}_{\text{sat}}\right\|$ which is the same as in vacuum, for convenience. Given these specifications of rectilinear initial and boundary conditions, raytracing proceeds as before.

Atmospheric delay modeling

Now, we describe how to model the interferometric atmospheric delay given the output of the raytracing procedure laid above.

Rigorous delay formulation

Table 1 summarizes the definitions of the intrinsic radio propagation quantities between any two points: vacuum distance: $D = \|\boldsymbol{r}_1 - \boldsymbol{r}_2\|$; radio length: $L = \int_{\boldsymbol{r}_1}^{\boldsymbol{r}_2} n\, dl$; and curve range: $R = \int_{\boldsymbol{r}_1}^{\boldsymbol{r}_2} 1\, dl$. Table 2 recapitulates the atmospheric delay and its components: total: $d = L - D = d^a + d^g$; along-path: $d^a = L - R = \int_{\boldsymbol{r}_1}^{\boldsymbol{r}_2} N\, dl$; and geometric atmospheric delay: $d^g = R - D$. For details, the reader is directed to Nikolaidou et al. (2020).

The interferometric quantities yield as the difference of the corresponding reflection and direct quantities, for example, interferometric vacuum distance: $D_i = D_r - D_d$; interferometric radio length: $L_i = L_r - L_d$; and interferometric curve range: $R_i = R_r - R_d$. The interferometric atmospheric delay follows from two equivalent formulations:

$$d_i = d_r - d_d = L_i - D_i \tag{13}$$

This definition is extended to the interferometric delay components, the along-path delay: $d_i^a = L_i - R_i$ and the geometric one: $d_i^g = R_i - D_i$. As before, the two parts make up the total delay, i.e., $d_i = d_i^a + d_i^g$ (Nikolaidou et al. 2020).

Finally, the atmospheric geometric delay can be further decomposed into the geometric-excess and the geometric-shift delays as $d_i^g = d_i^{g'} + d_i^{g''}$. This is possible with the introduction of a shifted vacuum delay D'_i :

Table 1 Definition of the propagation quantities

	Vacuum distance	Radio length	Curve range
(Generic)	$D = \|\boldsymbol{r}_1 - \boldsymbol{r}_2\|$	$L = \int_{\boldsymbol{r}_1}^{\boldsymbol{r}_2} n\, dl$	$R = \int_{\boldsymbol{r}_1}^{\boldsymbol{r}_2} 1 dl$
Direct	$D_d = \|\boldsymbol{r}_{\text{ant}} - \boldsymbol{r}_{\text{sat}}\|$	$L_d = \int_{\boldsymbol{r}_{ant}}^{\boldsymbol{r}_{sat}} n\, dl$	$R_d = \int_{\boldsymbol{r}_{\text{ant}}}^{\boldsymbol{r}_{\text{sat}}} 1\, dl$
Reflection	$D_r = \|\boldsymbol{r}_{\text{ant}} - \boldsymbol{r}_{\text{sfc}}\| + \|\boldsymbol{r}_{\text{sfc}} - \boldsymbol{r}_{\text{sat}}\|$	$L_r = \int_{\boldsymbol{r}'_{\text{sfc}}}^{\boldsymbol{r}_{\text{sat}}} n\, dl + \int_{\boldsymbol{r}_{\text{ant}}}^{\boldsymbol{r}'_{\text{sfc}}} n\, dl$	$R_r = \int_{\boldsymbol{r}'_{\text{sfc}}}^{\boldsymbol{r}_{\text{sat}}} 1\, dl + \int_{\boldsymbol{r}_{\text{ant}}}^{\boldsymbol{r}'_{\text{sfc}}} 1\, dl$
Interferometric	$D_i = D_r - D_d$	$L_i = L_r - L_d$	$R_i = R_r - R_d$

$$\begin{aligned} d_i^{g\prime} &= R_i - D_i' \\ d_i^{g\prime\prime} &= D_i' - D_i \end{aligned} \tag{14}$$

where

$$\begin{aligned} D_i &= \|\boldsymbol{r}_{\text{ant}} - \boldsymbol{r}_{\text{sfc}}\| + \|\boldsymbol{r}_{\text{sfc}} - \boldsymbol{r}_{\text{sat}}\| - \|\boldsymbol{r}_{\text{ant}} - \boldsymbol{r}_{\text{sat}}\| \\ D_i' &= \left\|\boldsymbol{r}_{\text{ant}} - \boldsymbol{r}_{\text{sfc}}'\right\| + \left\|\boldsymbol{r}_{\text{sfc}}' - \boldsymbol{r}_{\text{sat}}'\right\| - \left\|\boldsymbol{r}_{\text{ant}} - \boldsymbol{r}_{\text{sat}}'\right\| \end{aligned}. \tag{15}$$

So, while the ordinary vacuum delay D_i involves the vacuum reflection point, the shifted vacuum delay D_i' is obtained freezing the refracted reflection geometry (shifted specular point $\boldsymbol{r}_{\text{sfc}}'$ and apparent satellite direction $\Delta\hat{\boldsymbol{r}}_{\text{sfc}}'$) and undressing the atmosphere (i.e., nullifying the refractivity, $N = 0$).

The atmospheric geometric-shift delay is a consequence of the application of Snell's law at the refracted reflection point. It will maintain its magnitude even for small reflector heights, as it is largely formed by the angular refraction taking place above the receiving antenna. In contrast, the atmospheric geometric-excess delay corresponds to the deviation of the ray paths from straight-line segments. It may be assumed close to zero for sufficiently small reflector heights, as determined below.

Rectilinear delay formulation

In Table 3 we have adapted the rigorous definitions above (henceforth RI) for the two cases of rectilinear propagation (RG and RA); an overhead bar notation is used for distinction.

The RG vacuum distance equals the ordinary one used in the RI case, $\bar{D} = D$. In the RA approach, though, it equals the shifted vacuum distance, $\bar{D}' = D'$. The RG approach lacks any angular refraction effect and is subject only to linear refraction, albeit on a simplified ray path. The RA approach, on the other hand, includes both types of refraction, although ray bending is accounted in an all-or-nothing manner, only in the incident direction and it is not allowed to vary along the raypath as in the RI case. In both rectilinear cases, the curve range equals the respective vacuum distances, as there is no ray bending:

$$\begin{aligned} \bar{R} &= \bar{D}, \\ \bar{R}' &= \bar{D}'. \end{aligned} \tag{16}$$

The rectilinear models may seem overly simplistic, but it turns out a judicious combination proved accurate, as demonstrated by results below. We define a *rectilinear-mixed* (RM) model, denoted with double overhead bars.

Table 2 Definition of atmospheric delay and its components

	Total atmospheric delay	Along-path atmospheric delay	Geometric atmospheric delay
(Generic)	$d = L - D$ $d = d^a + d^g$	$d^a = L - R = \int_{\boldsymbol{r}_1}^{\boldsymbol{r}_2} N\, dl$	$d^g = R - D$
Direct	$d_d = L_d - D_d$ $d_d = d_d^a + d_d^g$	$d_d^a = L_d - R_d$	$d_d^g = R_d - D_d$
Reflection	$d_r = L_r - D_r$ $d_r = d_r^a + d_r^g$	$d_r^a = L_r - R_r$	$d_r^g = R_r - D_r$
Interferometric	$d_i = L_i - D_i$ $d_i = d_r - d_d$ $d_i = d_i^a - d_i^g$	$d_i^a = L_i - R_i$	$d_i^g = R_i - D_i$ $d_i^g = d_r^g - d_d^g$

Table 3 Definition of rectilinear propagation quantities

	Rectilinear geometric (RG)		Rectilinear apparent (RA)	
	Vacuum distance	Radio length	Vacuum distance	Radio length
Direct	$\bar{D}_d = \|\boldsymbol{r}_{\text{ant}} - \boldsymbol{r}_{\text{sat}}\|$	$\bar{L}_d = \int_{r_{\text{ant}}}^{r_{\text{sat}}} n\, ds$	$\bar{D}_d' = \left\|\boldsymbol{r}_{\text{ant}} - \boldsymbol{r}_{\text{sat}}'\right\|$	$\bar{L}_d' = \int_{\boldsymbol{r}_{\text{ant}}}^{\boldsymbol{r}_{\text{sat}}'} n\, ds$
Reflection	$\bar{D}_r = \|\boldsymbol{r}_{\text{ant}} - \boldsymbol{r}_{\text{sfc}}\| + \|\boldsymbol{r}_{\text{sfc}} - \boldsymbol{r}_{\text{sat}}\|$	$\bar{L}_r = \int_{\boldsymbol{r}_{\text{sfc}}}^{\boldsymbol{r}_{\text{sat}}} n\, ds + \int_{\boldsymbol{r}_{\text{ant}}}^{\boldsymbol{r}_{\text{sfc}}} n\, ds$	$\bar{D}_r' = \left\|\boldsymbol{r}_{\text{ant}} - \boldsymbol{r}_{\text{sfc}}'\right\| + \left\|\boldsymbol{r}_{\text{sfc}}' - \boldsymbol{r}_{\text{sat}}'\right\|$	$\bar{L}_r = \int_{\boldsymbol{r}_{\text{sfc}}'}^{\boldsymbol{r}_{\text{sat}}'} n\, ds + \int_{\boldsymbol{r}_{\text{ant}}}^{\boldsymbol{r}_{\text{sfc}}'} n\, ds$
Interferometric	$\bar{D}_i = \bar{D}_r - \bar{D}_d$	$\bar{L}_i = \bar{L}_r - \bar{L}_d$	$\bar{D}_i' = \bar{D}_r' - \bar{D}_d'$	$\bar{L}_i' = \bar{L}_r' - \bar{L}_d'$

Table 4 Definition of rectilinear interferometric atmospheric delays

	Rectilinear geometric	Rectilinear apparent	Rectilinear Mixed
Along-path	$\bar{d}_i^a = \bar{L}_i - \bar{R}_i$ $d_i^a = L_i - D_i$	$\bar{d}_i'^a = \bar{L}_i' - \bar{R}_i'$ $d_i'^a = L_i' - D_i'$	$\bar{\bar{d}}_i^a = \bar{\bar{L}}_i - \bar{\bar{R}}_i$ $\bar{\bar{d}}_i^a = \bar{\bar{L}}_i' - \bar{\bar{R}}_i'$ $\bar{\bar{d}}_i^a = \bar{\bar{d}}_i'^a$
Geometric	$\bar{d}_i^g = \bar{R}_i - \bar{D}_i$ $d_i^g = 0$	$\bar{d}_i'^g = \bar{R}_i' - \bar{D}_i'$ $d_i'^g = 0$	$\bar{\bar{d}}_i^g = \bar{\bar{R}}_i - \bar{\bar{D}}_i$ $\bar{\bar{d}}_i^{g\prime} = \bar{\bar{R}}_i - \bar{D}_i$ $\bar{\bar{d}}_i^{g\prime\prime} = \bar{D}_i' - \bar{D}_i$
Total	$\bar{d}_i = \bar{d}_i^a + \bar{d}_i^g$ $d_i = d_i^a$	$\bar{d}_i' = \bar{d}_i'^a + \bar{d}_i'^g$ $d_i' = d_i'^a$	$\bar{\bar{d}}_i = \bar{\bar{d}}_i^a + \bar{\bar{d}}_i^g$

It utilizes the RG vacuum distance in conjunction with the RA radio length and the RA curve range:

$$\begin{aligned} \bar{\bar{D}} &= \bar{D}, \\ \bar{\bar{R}} &= \bar{R}', \\ \bar{\bar{L}} &= \bar{L}'. \end{aligned} \tag{17}$$

Table 4 summarizes the definitions of the various rectilinear interferometric atmospheric delays and their components.

Where necessary, the atmospheric altimetry correction follows from half the rate of change of delay with respect to the sine of the elevation angle (Nikolaidou et al. 2020):

$$\Delta\bar{H} = -0.5\partial\bar{d}_i/\partial \sin e. \tag{18}$$

Results and discussion

Here, we assess results from rectilinear approach against rigorous raytracing. We assess first wave propagation quantities and later the derived atmospheric delays and altimetry corrections.

As atmospheric model source, we employed the COSPAR International Reference Atmosphere 1986 (CIRA-86) climatology (Chandra et al. 1990; Fleming et al. 1990); more specifically, file twp.lsn, available for download from https://ccmc.gsfc.nasa.gov/modelweb/atmos/cospar1.html. It provides temperature (0–120 km) and pressure (20–120 km) at 5-km intervals; surface pressure is obtained via hydrostatic integration. Temperature and pressure at any other sampling points are obtained via linear and log-linear interpolation, respectively.

In terms of computational cost, for an elevation angle of 5 degrees and a delay convergence tolerance of 10^{-6}m, the processing time decreases by 67%, from 0.45 s in RI to 0.15 s in RM, i.e., RM takes only one-third the time taken by RI.

Propagation quantities

We start by illustrating in Fig. 2 the discrepancy in interferometric vacuum distance, D_i. The rectilinear-geometric (RG) result, $\bar{D}_i$, is in near absolute agreement with that of RI. In contrast, rectilinear apparent (RA) result, $\bar{D}_i'$, falls short of D_i by an amount which is a consequence of angular refraction (ray bending angle, $\delta e = e' - e$). At zenith, all interferometric vacuum distances agree to $2H$. Their discrepancy increases at low elevation angles, reaching 6.5 cm at 5° elevation angle for a 10-m reflector height.

Next, Fig. 3 shows the discrepancy in interferometric curve range, R_i, among the various approaches. Contrary to the previous comparison, here the RG curve range, $\bar{R}_i$, has a large discrepancy with respect to RI. In this comparison, it is RA that best matches RI, $\bar{R}_i' \approx R_i$, as both are subject to angular refraction on the raypath. So, although the fictitious refracted satellite is very far from the actual satellite position, it is more representative for the calculation of the interferometric curve range. The agreement between RA and RI is not exact because rectilinear propagation neglects path-dependent incremental ray bending, accounting only for the total ray bending. The RA curve range degenerates to the respective (modified) vacuum distance, $\bar{R}_i' = \bar{D}_i'$.

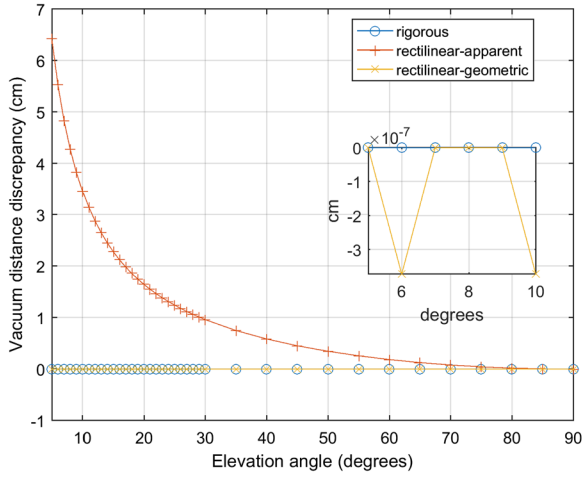

Fig. 2 Vacuum distance discrepancy as a function of satellite elevation angle (for a fixed 10-m reflector height)

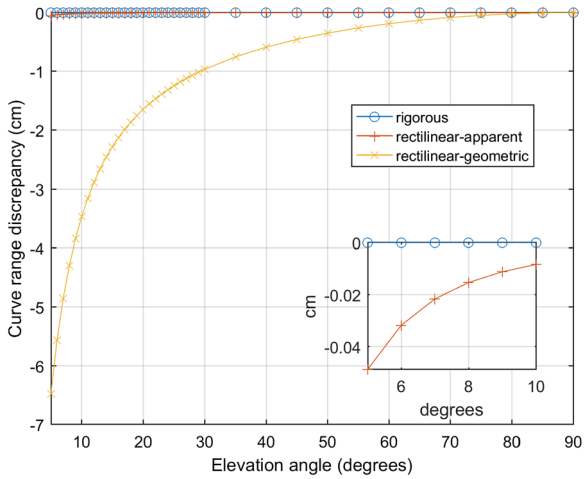

Fig. 3 Curve range discrepancy as a function of satellite elevation angle (for a fixed 10-m reflector height)

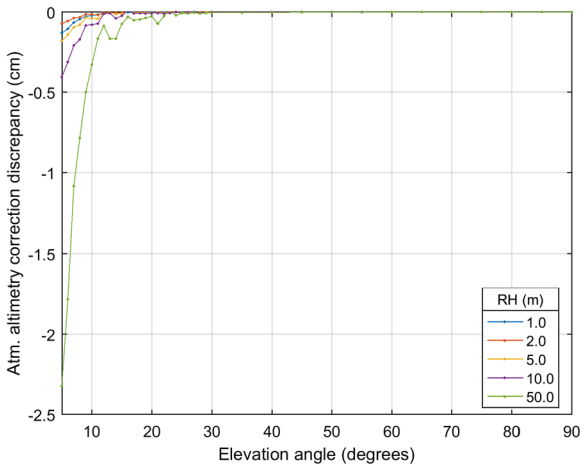

Fig. 5 Discrepancy in interferometric atmospheric altimetry correction between RM and RI formulations as a function of satellite elevation angle (for multiple reflector heights)

Last, the discrepancy in interferometric radio length L_i follows a similar pattern than that of the interferometric curve range (Fig. 3), with RI agreeing better with RA, $\bar{L}'_i$, than with RG, $\bar{L}_i$. This characteristic will be further analyzed below, in terms of the atmospheric delay.

In summary, RI vacuum distance is best approximated by RG while RI curve range and RI radio length are best approximated by RA. With this we justify the rectilinear-mixed (RM) approach (17), which borrows the best of each rectilinear models: RG $\left(\bar{\bar{D}}_i = \bar{D}_i\right)$ and RA $\left(\bar{\bar{L}}_i = \bar{L}'_i \text{ and } \bar{\bar{R}}_i = \bar{R}'_i\right)$.

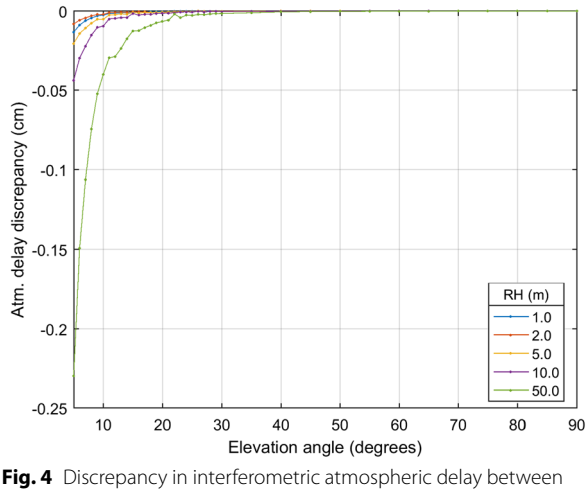

Fig. 4 Discrepancy in interferometric atmospheric delay between RM and RI formulations as a function of satellite elevation angle (for multiple reflector heights)

Total atmospheric delay and altimetry correction

In this section, we shall assess rectilinear results in terms of atmospheric delay and the resulting atmospheric altimetry correction. Figure 4 shows the discrepancy, $\bar{\bar{d}}_i - d_i$, in total interferometric atmospheric delay, between RM ($\bar{\bar{d}}_i = \bar{\bar{L}}_i - \bar{\bar{D}}_i$) and RI ($d_i = L_i - D_i$) approaches. For a 10-m reflector height, the agreement is excellent, having a maximum sub-mm discrepancy near the horizon. Further, it demonstrates that rigorous results (RI) can be approximated well by a judicious rectilinear propagation scheme (RM). It is remarkable that the effect of ray bending can be accurately represented by a straight line at the appropriate direction in the interferometric case.

The discrepancy in the resulting interferometric atmospheric altimetry correction (Fig. 5) follows a similar pattern than in the previous result, but scaled approximately by a factor of ten. The maximum discrepancy in atmospheric altimetry is found near the horizon, amounting to 0.4 cm for a 10-m reflector height. Both figures illustrate the proportional increase in the discrepancy with reflector height. For a reflector height of 20 m, the RM–RI agreement is better than 1 cm in altimetry correction for any elevation above 5 degrees; so the 20-m antenna height may be adopted as a threshold of validity for the assumption of near-surface conditions for the rectilinear model.

Atmospheric delay components

Figure 6 compares interferometric geometric atmospheric delay, across RI $\left(d_i^g = R_i - D_i\right)$ and RM $\left(\bar{\bar{d}}_i^g = \bar{\bar{R}}_i - \bar{\bar{D}}_i\right)$ approaches. The discrepancy $\bar{\bar{d}}_i^g - d_i^g$

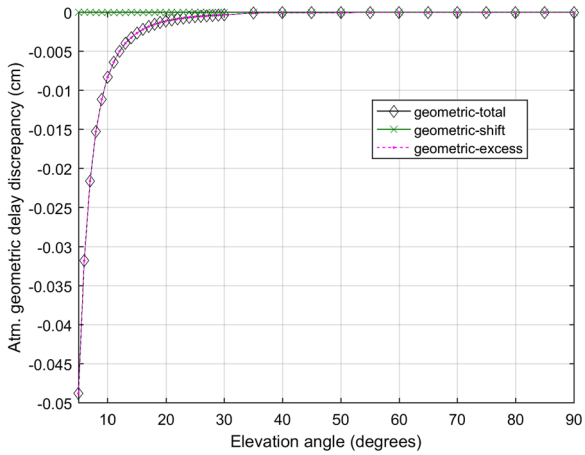

Fig. 6 Discrepancy in interferometric atmospheric geometric delay between RM and RI formulations as a function of satellite elevation angle (for a fixed 10-m reflector height)

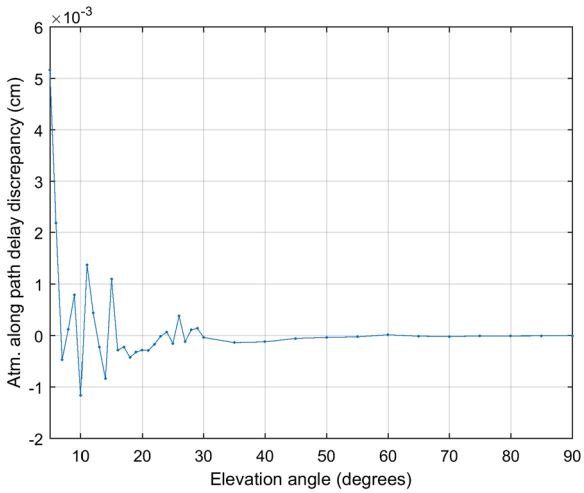

Fig. 7 Discrepancy in interferometric atmospheric along-path delay between RM and RI formulations as a function of satellite elevation angle (for a fixed 10-m reflector height)

converges to zero at zenith, where elevation bending is null, and it grows to at most 1 mm toward the horizon for a 10-m reflector height. Figure 4 demonstrates that the bulk of angular refraction is well captured by the atmospheric geometric-shift delay, the difference between RA and RG interferometric vacuum distances, $\bar{d}_i^{g''} = \bar{D}_i' - \bar{D}_i$. The present RM–RI discrepancy in geometric delay is dominated by the atmospheric geometric-excess delay, which also equals the RA–RI discrepancy in curve ranges: $\bar{d}_i^g - d_i^g = \bar{d}_i^{g'} - d_i^{g'} = \bar{R}_i' - R_i$. Thus, it follows from the incremental elevation bending present in rigorous raytracing but absent in the rectilinear approaches.

Figure 7 shows the discrepancy, $\bar{d}_i^a - d_i^a$, in interferometric along-path atmospheric delay, across RI $\left(d_i^a = L_i - R_i\right)$ and RM $\left(\bar{\bar{d}}_i^a = \bar{\bar{L}}_i - \bar{\bar{R}}_i\right)$ cases. The agreement is even better (at 50 μm level), with discrepancy values more randomly distributed, resembling numerical noise (likely caused by interpolation in the CIRA atmospheric model).

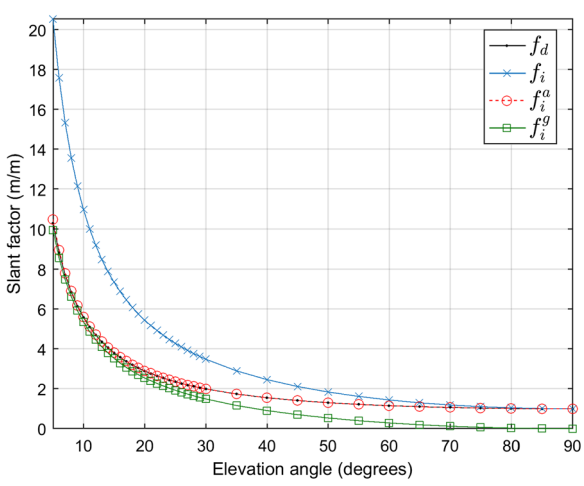

Fig. 8 Slant factors for the direct and interferometric—total and components—signals as a function of satellite elevation angle (for a fixed 10-m reflector height)

Slant factors

For a better comparison to the standard approach reported in the literature, based on mapping functions, we provide an analysis based on slant factors, $f = d/d^z$, defined as the ratio between slant delay and zenith delay at a particular elevation angle. Slant factors computed from direct raytracing are the input data for developing mapping function models, such as the Global Mapping Function (GMF) (Boehm et al. 2006), after fitting to a particular functional expression valid over a given space–time domain (Urquhart et al. 2012).

The direct slant factor is defined as $f_d = d_d/d_d^z$, where the direct zenith delay is that at the antenna: $d_d^z = d_{\text{ant}}^z$. The interferometric slant factor, $f_i = d_i/d_i^z$, uses the total interferometric zenith delay, $d_i^z = 2\left(d_{ant}^z - d_{sfc}^z\right)$, which is twice the zenith delay difference across antenna and surface. The slant factors for interferometric components $f_i = f_i^a + f_i^g$ are computed similarly, as $f_i^a = d_i^a/d_i^z$ and $f_i^g = d_i^g/d_i^z$ for along-path and geometric terms, respectively.

Figure 8 shows the slant factors defined above. They all follow the exponential decay of delay with elevation angle. However, at the lowest elevation angle (5 degrees) the interferometric slant factor measures twice the direct one (20.47 m/m vs. 10.29 m/m). At zenith, where angular

refraction is null, they both converge to unity. At low elevation angle, though, using a direct mapping function will underestimate the interferometric delay systematically with decreasing elevation angle by up to 50%.

In relation to the components, the interferometric along-path slant factor resembles the direct slant factor, $f_i^a \approx f_d$. They are both related to the thickness of atmospheric layers, albeit different ones: respectively, the inner and outer ones, below and above the antenna. Furthermore, the direct slant factor $f_d = f_d^a + f_d^g$ also involves a weighting of the layer slant distances by refractivity in the integrand of $\int Ndl$, as well as a minor contribution from the direct atmospheric geometric delay, f_d^g. The interferometric geometric slant factor f_i^g approaches the along-path one f_i^a at low elevations, e.g., 9.97 m/m vs. 10.51 m/m at 5° elevation angle, but converges to zero at zenith due to the absence of bending.

Finally, it should be emphasized that mapping functions developed for GNSS positioning, such as the GMF, are supposed to agree only with the direct slant factors, as in fact it does the agreement with our results is within 2% at 5° (not shown). However, correcting for the atmospheric interferometric delay in GNSS-R using GMF or a similar mapping functions will introduce an exponentially increasing bias with elevation angle. The remaining geometric-shift atmospheric delay, which is a result of Snell's law on the refracted specular point, cannot be captured using only the direct or LOS propagation effects, and would require a model for the angular refraction.

Conclusions

A simplification of the rigorous interferometric raytracing approach (RI) was carried out, imposing a rectilinear ray propagation model for GNSS reflectometry (GNSS-R) applications. Two initial variants were developed, considering the apparent (refracted) and the geometric (vacuum) satellite directions. The rectilinear-geometric (RG) agreed with the rigorous (RI) for the vacuum distance, while the rectilinear-apparent (RA) agreed with RI for the radio length. Both RG and RA had poor performance in terms of atmospheric delays, though.

Upon combination of the best matching aspect of the two above, RG and RA, we defined a third variant, the rectilinear-mixed (RM) model. It demonstrated excellent agreement in the interferometric atmospheric delay, both in total value and in all components (along-path and geometric). GNSS-R altimetry corrections can, therefore, be predicted by performing a single rigorous raytracing in the direct or line-of-sight direction to determine the ray bending, followed by two rectilinear raytracings in the direct and reflection directions.

The rectilinear models demonstrated for the interferometric atmospheric delay allow for faster and more efficient raytracing, as the reflection three-point boundary-value problem (satellite–surface–antenna) can be replaced for an easier two-point problem. Thus, existing raytracing software can be adapted more easily for ground-based GNSS-R applications. The simplifications demonstrated here also pave the way for the future development of more convenient closed-form expressions.

Another key demonstration is that mapping functions developed for GNSS positioning, or even a direct raytracing procedure, cannot be reused for GNSS-R purposes without adaptations. The interferometric atmospheric delay is induced by the atmosphere both above and below the receiver, roughly corresponding to its angular refraction and linear refraction components. At low elevation angles, where the interferometric delay components are similar, direct-only mapping functions will underestimate the total delay by nearly half. In the current study, however, we showed how the interferometric delay and its components can be deduced with a direct-only raytracing procedure by employing a judicious combination of two simpler rectilinear models for the raypath.

Abbreviations

GNSS-R: Global Navigation Satellite System Reflectometry; RA: Rectilinear apparent; RG: Rectilinear geometric; RM: Rectilinear-mixed; RI: Rigorous raytracing approach.

Acknowledgements

Not applicable.

Authors' contributions

FGN and TN conceived the idea. FGN and TN developed the theory and performed the computations. MCS and SDPW verified the analytical methods. SDPW provided experimental data. FGN and TN wrote the manuscript. MCS contributed to the final version of it. All authors provided critical feedback and helped shape the research. All authors read and approved the final manuscript.

Funding

FGN acknowledges funding from CNPq (Conselho Nacional de Desenvolvimento Científico e Tecnológico; 457530/2014-6, 433099/2018-6) and Fapergs (Fundação de Amparo à Pesquisa do Estado do Rio Grande do Sul; 26228.414.42497.26062017). TN acknowledges funding from Mitacs (Grant No. IT11988).

Availability of data and materials

No external datasets were used for this study. The study uses simulation results.

Ethics approval and consent to participate

Not applicable.

Consent for publication

Not applicable.

Competing interests

The authors declare that they have no competing interests.

Author details

[1] Department of Geodesy and Geomatics Engineering, University of New Brunswick, Fredericton, Canada. [2] National Oceanography Centre, Liverpool,

UK. [3] Department of Geodesy, Federal University of Rio Grande do Sul, Porto Alegre, Brazil.

Received: 14 October 2019 Accepted: 24 May 2020
Published online: 02 July 2020

References

Anderson KD (2000) Determination of water level and tides using interferometric observations of GPS signals. J Atmos Ocean Technol 17:1118–1127. https://doi.org/10.1175/1520-0426(2000)017%3c1118:DOWLAT%3e2.0.CO;2

Bender M, Dick G, Ge M et al (2011) Development of a GNSS water vapour tomography system using algebraic reconstruction techniques. Adv Sp Res 47:1704–1720. https://doi.org/10.1016/J.ASR.2010.05.034

Boehm J, Niell A, Tregoning P, Schuh H (2006) Global Mapping Function (GMF): a new empirical mapping function based on numerical weather model data. Geophys Res Lett 33:L07304. https://doi.org/10.1029/2005GL025546

Born M, Wolf E (1999) Principles of optics Electromagnetic theory of propagation, interference and diffraction of light, 7th expand. Cambridge University Press

Cardellach E, Fabra F, Nogués-Correig O et al (2011) GNSS-R ground-based and airborne campaigns for ocean, land, ice, and snow techniques: application to the GOLD-RTR data sets. Radio Sci. https://doi.org/10.1029/2011RS004683

Chandra S, Fleming EL, Schoeberl MR, Barnett JJ (1990) Monthly mean global climatology of temperature, wind, geopotential height and pressure for 0–120 km. Adv Space Res 10(6):3–12. https://doi.org/10.1016/0273-1177(90)90230-W

Fabra F, Cardellach E, Rius A et al (2012) Phase altimetry with dual polarization GNSS-R over sea ice. IEEE Trans Geosci Remote Sens 50:2112–2121. https://doi.org/10.1109/TGRS.2011.2172797

Fleming EL, Chandra S, Barnett JJ, Corney M (1990) Zonal mean temperature, pressure, zonal wind and geopotential height as functions of latitude. Adv Space Res 10(12):11–59. https://doi.org/10.1016/0273-1177(90)90386-E

Hopfield HS (1969) Two-quartic tropospheric refractivity profile for correcting satellite data. J Geophys Res. 74(18):4487–4499

Jin S, Cardellach E, Xie F (2014) GNSS remote sensing theory, methods and applications. Springer, Netherlands

Larson KM, Ray RD, Nievinski FG, Freymueller JT (2013) The accidental tide gauge: a GPS reflection case study from Kachemak Bay, Alaska. IEEE Geosci Remote Sens Lett. https://doi.org/10.1109/LGRS.2012.2236075

Larson KM, Ray RD, Williams SDP et al (2017) A 10-year comparison of water levels measured with a geodetic GPS receiver versus a conventional tide gauge. J Atmos Ocean Technol 34:295–307. https://doi.org/10.1175/JTECH-D-16-0101.1

Nafisi V, Urquhart L, Santos MC et al (2012) Comparison of ray-tracing packages for troposphere delays. IEEE Trans Geosci Remote Sens 50:469–481. https://doi.org/10.1109/TGRS.2011.2160952

Nievinski FG, Larson KM (2014) Forward modeling of GPS multipath for near-surface reflectometry and positioning applications. GPS Solut 18:309–322. https://doi.org/10.1007/s10291-013-0331-y

Nievinski FG, Santos MC (2010) Ray-tracing options to mitigate the neutral atmosphere delay in GPS. Geomatica 64:191–207

Nikolaidou T, Santos CM, Williams DPS, Geremia-Nievinski F (2020) Raytracing atmospheric delays in ground-based GNSS reflectometry. J Geod. https://doi.org/10.1007/s00190-020-01390-8

Nilsson T, Böhm J, Wijaya DD et al (2013) Path delays in the neutral atmosphere. Springer, Berlin, pp 73–136

Rohm W, Bosy J (2009) Local tomography troposphere model over mountains area. Atmos Res 93:777–783. https://doi.org/10.1016/J.ATMOSRES.2009.03.013

Roussel N, Frappart F, Ramillien G et al (2014) Simulations of direct and reflected wave trajectories for ground-based GNSS-R experiments. Geosci Model Dev. https://doi.org/10.5194/gmd-7-2261-2014

Saastamoinen J (1972) Atmospheric correction for the troposphere and stratosphere in radio ranging satellites. American Geophysical Union (AGU), Washington, D. C, pp 247–251

Santamaría-Gómez A, Watson C (2017) Remote leveling of tide gauges using GNSS reflectometry: case study at Spring Bay, Australia. GPS Solut 21:451–459. https://doi.org/10.1007/s10291-016-0537-x

Santamaría-Gómez A, Watson C, Gravelle M et al (2015) Levelling co-located GNSS and tide gauge stations using GNSS reflectometry. J Geod 89:241–258. https://doi.org/10.1007/s00190-014-0784-y

Semmling AM, Schmidt T, Wickert J et al (2012) On the retrieval of the specular reflection in GNSS carrier observations for ocean altimetry. Radio Sci. https://doi.org/10.1029/2012RS005007

Treuhaft RN, Lowe ST, Zuffada C, Chao Y (2001) 2-cm GPS altimetry over Crater Lake. Geophys Res Lett 28:4343–4346. https://doi.org/10.1029/2001GL013815

Urquhart L, Nievinski FG, Santos MC (2012) Ray-traced slant factors for mitigating the tropospheric delay at the observation level. J Geod 86:149–160. https://doi.org/10.1007/s00190-011-0503-x

Williams SDP, Nievinski FG (2017) Tropospheric delays in ground-based GNSS multipath reflectometry—experimental evidence from coastal sites. J Geophys Res Solid Earth 122:2310–2327. https://doi.org/10.1002/2016JB013612

Zavorotny VU, Gleason S, Cardellach E, Camps A (2014) Tutorial on remote sensing using GNSS bistatic radar of opportunity. IEEE Geosci Remote Sens Mag 2:8–45. https://doi.org/10.1109/MGRS.2014.2374220

Publisher's Note